Atmospheric
Measurement
Techniques
Open Access
Discussions

Synergistic angular and spectral estimation of aerosol properties using CHRIS/PROBA-1 and simulated Sentinel-3 data

W. H. Davies and P. R. J. North

College of Science, Swansea University, Singleton Park, Swansea, SA2 8PP, UK

Correspondence to: W. H. Davies (w.h.davies@uclmail.net)

Discussion Paper | Discussion Paper | Discussion Paper | Discussion Paper |

AMTD

7, 5381–5422, 2014

Synergistic aerosol estimation from simulated Sentinel-3 data

W. H. Davies and P. R. J. North

Title Page

Abstract | Introduction

Conclusions | References

Tables | Figures

|◄ | ►|

◄ | ►

Back | Close

Full Screen / Esc

Printer-friendly Version

Interactive Discussion

W. H. Davies and
P. R. J. North

Title Page

Abstract   Introduction

Conclusions   References

Tables   Figures

◄   ►►

◄   ►

Back   Close

Full Screen / Esc

Printer-friendly Version

Interactive Discussion

Abstract

A method has been developed to estimate Aerosol Optical Depth (AOD), Fine Mode Fraction (FMF) and Single Scattering Albedo (SSA) over land surfaces using simulated Sentinel-3 data. The method uses inversion of a coupled surface/atmosphere radiative transfer model, and includes a general physical model of angular surface reflectance. An iterative process is used to determine the optimum value of the aerosol properties providing the best fit of the corrected reflectance values for a number of view angles and wavelengths with those provided by the physical model. A method of estimating AOD using only angular retrieval has previously been demonstrated on data from the ENVISAT and PROBA-1 satellite instruments, and is extended here to the synergistic spectral and angular sampling of Sentinel-3 and the additional aerosol properties. The method is tested using hyperspectral, multi-angle Compact High Resolution Imaging Spectrometer (CHRIS) images. The values obtained from these CHRIS observations are validated using ground based sun-photometer measurements. Results from 22 image sets using the synergistic retrieval and improved aerosol models show an RMSE of 0.06 in AOD, reduced to 0.03 over vegetated targets.

1 Introduction

Limited understanding of atmospheric aerosol composition, distribution and function contributes the largest uncertainty to current estimates of Radiative Forcing (RF) and thereby to the uncertainty in future climate predictions (IPCC, 2013). The World Meteorological Organization (WMO) established the Global Climate Observing System (GCOS) in 1992 to focus on satellite observations in order to provide better aerosol products leading to a reduction in climate uncertainty. GCOS has a target accuracy of 0.01 for AOD and 0.02 for SSA (GCOS, 2006). In this paper we aim to use recent improvements in the definition of common aerosol components (Holzer-Popp et al., 2013) to show that better atmospherically corrected surface reflectance, Aerosol

Optical Depth (AOD), Fine Mode Fraction (FMF) and Single Scattering Albedo (SSA) should be possible using synergistic retrieval from new satellite observations.

In summarising the drivers of climate change, the Intergovernmental Panel on Climate Change (IPCC) found that there is a negative RF from most aerosols with a total aerosol effect of between −1.9 and −0.1 W m^{-2} (IPCC, 2013). However, the effect of aerosols is highly variable – aerosols that scatter have a cooling or negative forcing effect whereas absorbing aerosols have a warming or positive forcing effect (Bergstrom et al., 2002). SSA is the ratio of scattering to total extinction. SSA determines whether the radiative forcing of aerosols is negative or positive whereas the phase function and the AOD determine the magnitude of the forcing. A low value of SSA implies a high level of absorption, and conversely a high value of SSA implies a high degree of scattering and a low level of absorption (Dubovik et al., 2002). In addition to the direct effect, the value of SSA can also have an impact on cloud formation. The INDOEX experiment demonstrated that solar absorption by aerosols reduced day time cloud coverage over the Indian Ocean (Ackerman et al., 2000). According to Kazadzis et al. (2010), SSA may be the most significant uncertainty in current modelling of how aerosol forcing affects the climate. Recent reviews of retrieval of aerosol properties from existing satellites are found in Kokhanovsky and DeLeeuw (2009), Kokhanovsky et al. (2010), de Leeuw et al. (2013) and Holzer-Popp et al. (2013).

As part of the Global Monitoring for Environment and Security (GMES) programme, the European Space Agency (ESA) is expected to launch the first two Sentinel-3 satellites before the end of 2015 (ESA-Earth-Online, 2014). The Sea and Land Surface Temperature Radiometer (SLSTR) and Ocean and Land Colour Instrument (OLCI) on Sentinel-3 are an improvement on the Advanced Along Track Scanning Radiometer (AATSR) and the Medium Resolution Imaging Spectrometer (MERIS) on the ENVISAT satellite with better spatial resolution, wider swath coverage and more bands (Donlon et al., 2012). A multi-angle method of retrieving surface reflectance has previously been demonstrated on data from the CHRIS and AATSR satellite instruments (North, 2002; Bevan et al., 2012; Davies et al., 2010), and has been extended to use synergistic

Synergistic aerosol estimation from simulated Sentinel-3 data

W. H. Davies and
P. R. J. North

Title Page

Abstract | Introduction

Conclusions | References

Tables | Figures

|◄ | ►|

◄ | ►

Back | Close

Full Screen / Esc

Printer-friendly Version

Interactive Discussion

spectral and angular information from MERIS and AATSR on ENVISAT (North et al., 2008, 2010), and OLCI and SLSTR on Sentinel-3 (North and Heckel, 2012).

Here we develop and test an experimental method for estimating AOD, FMF and SSA from simulated Sentinel-3 and real CHRIS data. The method explores the synergistic use of both SLSTR and OLCI using the multi-angle method and a spectral method respectively to provide more constraints for the retrieval (North et al., 2008). The method is tested using the 6S radiative transfer model (Vermote et al., 1997a) to generate simulated Sentinel-3 Top Of Atmosphere (TOA) radiances. Real CHRIS data are used to simulate Sentinel-3 data, and ground based sun-photometer measurements are used to validate the method. Unless stated otherwise, all AOD values are at 0.55 µm and all SSA values are at 0.87 µm.

2   Satellite instruments

2.1   SLSTR/Sentinel-3

Like AATSR, SLSTR is a dual-angle instrument with a nadir view and an oblique view at an angle of approximately 55° through the atmosphere. However on SLSTR the oblique view is to the rear to allow both SLSTR and OLCI to have a clear view to the sun for calibration purposes. It has a nadir swath of 1400 km and a dual view swath of 740 km. There is an improved spatial resolution of 500 m in the visible and Short Wave InfraRed (SWIR) channels and an additional band useful for aerosol retrieval centered at 2.25 µm. There is also an additional channel centered at 1.375 µm but this is excluded in the aerosol retrieval because of atmospheric absorption by water vapour. The 5 bands used are listed in Table 1. Scanner calibration using black body cavities is performed every second scan and visible channel gain calibration is performed once per orbit (Donlon et al., 2012).

Synergistic aerosol estimation from simulated Sentinel-3 data

W. H. Davies and
P. R. J. North

Title Page

Abstract | Introduction

Conclusions | References

Tables | Figures

|◄ | ►|

◄ | ►

Back | Close

Full Screen / Esc

Printer-friendly Version

Interactive Discussion

2.2 OLCI/Sentinel-3

OLCI is a push-broom instrument with 21 spectral channels covering the same range as MERIS with a spatial resolution of 300 m. Only 18 bands are used in the retrieval – the bands centred at the following wavelengths are excluded because of atmospheric absorption: 764.375 nm, 767.5 nm and 940 nm. The bands used are listed in Table 1. There is an improved global coverage compared to MERIS of less than 4 days over ocean and less than 3 days over land (assuming only 1 satellite). The swath of 1270 km overlaps with SLSTR which facilitates synergistic retrieval and is tilted westwards to mitigate contamination from sun-glint. Calibration is performed at the southern terminator crossing with dark current calibration and radiometric calibration in the first orbit in sequence and then in the following orbit dark current calibration and spectral calibration (Donlon et al., 2012).

2.3 CHRIS/PROBA-1

CHRIS is a multi-angle instrument which acquires images at a high spatial resolution (17 or 34 m), and is a hyper-spectral instrument offering a subset of 18 to 62 spectral bands in the optical region between 400 and 1050 nm. CHRIS acquires up to 5 images of the target area with a swath width of 13 km. The viewing zenith angles are nominally given as 55° and 36° in the backwards and forwards direction, and at nadir. There are a range of modes of data that can be selected for specific applications (Davies et al., 2010). In this data set, only modes 1 and 5 are used – mode 5 for the Gilching site and mode 1 for all the other target sites. The 18 bands used are listed in Table 1.

The reliability of the radiance measurements from the CHRIS instrument are dependent on a number of sources of uncertainty. This uncertainty in the satellite values, combined with the uncertainty in the retrieval process is transmitted through to errors in the properties that are to be estimated. One such source of instrument uncertainty is regarding the pointing of CHRIS to the target which leads to the images being misaligned. As well as the alignment of the spacecraft there are also timing errors in computing the

earth's rotation and calibration errors on inertia ratio and wheel axis which affect the accuracy of the pointing during the acquisition (Davidson and Vuilleumier, 2004). Radiometric uncertainties for this push-broom instrument come from the response of the Charge Coupled Device (CCD), the telescope and the spectrometer. There is also the effect of instrument temperature on the width of the slit (Gómez-Chova et al., 2008). Other causes of calibration problems are the mirror distortions which affect the spatial resolution, temperature related changes in the prism refractive index, and non uniform response from the Solar Calibration Device (SCD) (Cutter and Lobb, 2004). An example CHRIS image over Lake Argyle, Australia is displayed in Fig. 1.

3 Retrieval method

3.1 Overview

The retrieval is an iterative process: (1) The TOA Radiance measurements are transformed using 6S (Vermote et al., 1997a), along with an estimated value for the aerosol properties, to estimate surface reflectance. (2) An error metric is calculated based on fit of this surface reflectance set (R_{surf}) to a model of idealised land surface angular and spectral variation. (3) The aerosol estimate is refined, and steps 1 and 2 repeated until convergence, based on minimisation of the error metric.

3.2 Multi-angle model

The model – Eq. (1), is developed and justified in North et al. (1999). The inversion requires a minimum of two view angles, and a minimum of two wavelengths, but may be applied to the full set of CHRIS viewing angles and any waveband set (Davies et al., 2010).

$$R_{ang}(\lambda, \theta_v) = (1 - D(\lambda))P(\theta_v)\omega(\lambda) + \frac{\gamma\omega(\lambda)}{1 - g}(D(\lambda) + g(1 - D(\lambda))) \tag{1}$$

where

$$g = (1 - \gamma)\omega(\lambda)$$

λ is the wavelength, θ_v the view direction, $\omega(\lambda)$ the Lambertian scattering albedo, $P(\theta_v)$ the aggregate single scattering phase function, $D(\lambda)$ is the fraction of downwelling diffuse light and γ represents the probability of escape from the surface without further scattering. The set of free parameters $\omega(\lambda)$ and $P(\theta_v)$ are found by inversion.

3.3 Spectral model

Here we extend the method to make use of spectral information in addition to angular. For single angle viewing we use a spectral signature to isolate the aerosol scattering from the surface reflectance. We identify a set of surfaces with known reflectance and assuming an atmospheric profile, we fit the atmospherically corrected surface reflectance with the assumed target reflectance. Similar approaches have been used in aerosol retrieval for CHRIS (Guanter et al., 2005) and for MERIS (North et al., 2008; von Hoyningen-Huene et al., 2011).

The assumed target reflectance is represented as a linear mixture of a set of spectra:

$$R_{spec}(\lambda) = c_{vg}\rho_{vg}(\lambda) + c_{vd}\rho_{vd}(\lambda) + c_{vo}\rho_{vo}(\lambda) + c_s\rho_s(\lambda) + c_a\rho_a(\lambda) \tag{2}$$

where c_{vg} is the fractional coverage of green vegetation and ρ_{vg} is the corresponding surface reflectance of the input spectra and is a function of wavelength. Similarly, c_{vd} and ρ_{vd} are the fractional coverage and spectra for dry grass, c_{vo} and ρ_{vo} for other vegetation, c_s and ρ_s for soil and c_a and ρ_a for arid soil (Baldridge et al., 2009; Vermote et al., 1997a). The OLCI spectra are listed in Table 3, and CHRIS spectra in Table 4.

The metric for the single angle spectral retrieval is given by Eq. (3).

$$E_{spec} = \frac{\sum_{\lambda=1}^{18} w_\lambda [R_{surf}(\lambda) - \rho_{spec}(\lambda)]^2}{\sum_{\lambda=1}^{18} w_\lambda} \tag{3}$$

W. H. Davies and
P. R. J. North

where λ is the wavelength and w_λ is the per-band weighting factor. The per-band weighting factor values are normalised according to Eq. (4). By experiment, lowest error was found with a weighting of of 1.5/18 for the first wavelength, and a compensating 0.5/18 for the last (infra red) wavelength, and unity for all other wavelengths.

$$\sum_{\lambda=1}^{18} w_\lambda = 1 \tag{4}$$

3.4 Surface reflectance estimation

The estimated surface reflectance (R_{surf}) is calculated from the TOA radiance measurements at each iteration using a look-up table (LUT) of coefficients determined by 6S, and using aerosol properties determined under the ESA Aerosol CCI definitions (de Leeuw et al., 2013).

3.4.1 Atmospheric LUT coefficients

The calculation to determine surface reflectance from top of atmosphere radiance uses Eqs. (5) and (6) (Vermote et al., 1997b).

$$y = x_a \cdot I_{toa} - x_b \tag{5}$$
$$R_{surf} = y/[1.0 + x_c \cdot y] \tag{6}$$

where I_{toa} is the TOA radiance, R_{surf} is the atmospherically corrected surface reflectance, x_a, x_b, and x_c are calculated by 6S as part of the atmospheric correction process. x_a is the coefficient for converting between radiance and reflectance. x_b is the coefficient for atmospheric reflectance corrected for transmission effects and x_c is the coefficient for multiple interactions.

3.4.2 Uncertainty estimate

The uncertainty in R_{surf} is given by Eq. (7). From Eqs. (5) and (6) we get Eqs. (8) and (9). Taking the derivative of Eq. (8) with respect to I_{toa} we get Eq. (10) where M is given by Eq. (11).

$$\delta R_{surf} = \left(\frac{\delta R_{surf}}{\delta I_{toa}}\right)\delta I_{toa} \tag{7}$$

$$R_{surf} = \frac{x_a I_{toa} - x_b}{1 + x_c(x_a I_{toa} - x_b)} \tag{8}$$

$$I_{toa} = \frac{R_{surf}}{x_a(1 - x_c R_{surf})} + \frac{x_b}{x_a} \tag{9}$$

$$\sigma_{surf}^2 = \frac{x_a^2}{M^4}\sigma_i^2 \tag{10}$$

$$M = 1 + x_c(x_a I_{toa} - x_b) \tag{11}$$

If σ_i is the standard deviation of the error in the TOA radiance measurements then the fractional error in I_{toa} is given by Eq. (12) (β_i has the value 0.05 for CHRIS).

$$\beta_i = \frac{\sigma_i}{I_{toa}} \tag{12}$$

Substituting for σ_i we get Eq. (13).

$$\sigma_{surf}^2 = \beta_i^2 \frac{x_a^2}{M^4} I_{toa}^2 \tag{13}$$

3.4.3 Aerosol model set

The original method for CHRIS retrieval (Davies et al., 2010) retrieved a single unknown, AOD. Here we develop the method to retrieve four unknowns: AOD at

a reference wavelength (0.55 µm) and three components of aerosol mixture (the fourth component is implicit since all four must sum to 100 %). The four components are non-spherical dust, sea salt, weakly absorbing and strongly absorbing (de Leeuw et al., 2013). A full grid of AOD and mixture values in steps of 20 % is used in a LUT based approach giving a total of 560 points. The log-normal parameters and their associated mid-visible indices of refraction are listed in Table 2. Ten values of AOD are used from 0.01 to 0.46 in intervals of 0.05 – the range has been chosen to enclose that from the CHRIS data set. The retrieval process iterates through all the values in the grid, and the AOD/mix with the best fit is the solution.

For the CHRIS multi-angle viewing, the least-squares method is modified in order to take account of the need to propagate the uncertainties through to the resulting estimates. The approach of Diner et al. (2008) is adopted for the modified error metric which is given by Eq. (15).

3.5 Retrieval of surface reflectance and aerosol

An iterative search for the optimum aerosol model and optical depth is performed, by minimising the difference between the modeled and measured surface reflectance using a metric combining the angular and spectral constraints:

$$R_{mod} = R_{ang} + kR_{spec} \tag{14}$$

For a given aerosol model, the Powell and Brent methods (Press et al., 1992) are used to determine the parameters which minimise the constraint (15) such that E_{min} is the minimised value of E_{mod}.

$$E_{mod} = \sum_{\theta_v=1}^{5} \sum_{\lambda=1}^{18} \frac{[R_{surf}(\lambda, \theta_v) - R_{mod}(\lambda, \theta_v)]^2}{\sigma_{surf}^2 + \sigma_{mod}^2} \tag{15}$$

where λ is the wavelength and θ_v the view direction, and σ_{surf}^2 is given by Eq. (13). The error in R_{mod} is characterised by using simulated data from 36 sets of conditions.

The error variance at each view angle/wavelength combination is given by Eq. (16).

$$\sigma_{\mathrm{mod}}^2 = \frac{1}{n} \sum_{s=1}^{n} [R_{\mathrm{sim}}(\lambda, \theta_v, s) - R_{\mathrm{mod}}(\lambda, \theta_v, s)]^2 \qquad (16)$$

where $n = 36$, giving estimates of σ_{mod}^2 for each view angle/wavelength combination. For synergistic retrieval, the spectral and angular retrievals are run separately as a first iteration in order to calculate a normalising scaling factor k giving equal weighting to anglar and spectral metrics.

3.6 Error estimate in AOD

Values of the error metric E_{mod} bounding the minimum value are used to compute a parabolic fit, represented by the coefficients in Eq. (17) (Diner et al., 2008).

$$\ln(E_{\mathrm{mod}}) = A + B\tau + C\tau^2 \qquad (17)$$

and the uncertainty (σ_τ) in τ_{best} – the value of AOD that minimises E_{mod} is given by Eq. (18) (Diner et al., 2008).

$$\sigma_\tau = \sqrt{\frac{\ln\left(1 + \frac{1}{E_{\mathrm{min}}}\right)}{C}} \qquad (18)$$

The uncertainty in the retrieved mixture is calculated using the associated SSA value. Eqs. (17) and (18) are used again but substituting SSA for AOD. The uncertainty values for SSA are also used for the FMF estimates calculated from the same retrieved mixture.

4 Test datasets

4.1 Simulated data

Simulated data were generated to provide an initial test of the inversion. Simulated SLSTR and OLCI TOA radiances are generated by running 6S in forward mode using the 560 sets of AOD/mix, other parameters for the simulation are as follows with the geometry taken from one of the CHRIS image sets: Solar Zenith Angle (SZA) – 15.1°, Solar Azimuth Angle (SAA) – 95.3°, View Zenith Angle (VZA) – 7.25° for nadir, and 55° for the oblique view, View Azimuth Angle (VAA) – 316.12°, month – 11, day – 9, atmosphere – Tropical, altitude – 150 m and surface type – lambertian vegetation. The bands are listed in Table 1. The AOD, FMF and SSA values from the retrieval (Estimated AOD, FMF or SSA) are compared with the values from the generation of each TOA set (True AOD, FMF or SSA).

4.2 CHRIS data

Twenty two image sets were used from six different sites These are listed in Table 5 together with the number of image sets processed from that site, the type of land cover, the aerosol model used in the original method, the date range of the sets and the range of AOD as measured by the photometers (Davies et al., 2010). A subset of 18 bands from CHRIS were chosen to correspond with a subset of the bands from OLCI and SLSTR, and are listed in Table 1.

This represents all available archived CHRIS data suitable for testing. Further image sets were rejected for a variety of reasons: (i) no AERONET time/space coincidence; (ii) no acquisition of multi-angular data (iii) adequate meta-data for view geometry (iv) insufficient co-registered, cloud-free pixels visible in all views. (v) In addition, for testing FMF and SSA, the AOD at 440 nm must be > 0.2. (vi) No retrieval was also made if the retrieval failed the E_{min} threshold test. (vii) For use of the spectral constraint, a further

Title Page

Abstract | Introduction

Conclusions | References

Tables | Figures

|◄ | ►|

◄ | ►

Back | Close

Full Screen / Esc

Printer-friendly Version

Interactive Discussion

threshold of mean NDVI > 0.4 was used to isolated vegetated or partially vegetated scenes.

5 Results

5.1 AOD from simulated data

The AOD values retrieved from each of the 560 TOA radiance sets using the synergy method are compared with the true values in Fig. 3. The red dotted line represents where the 1 : 1 relationship would be, and the blue solid line represents the fitted trend line. The RMSE between true and estimated values is 0.03 and r^2 is 0.97. The regression coefficients are 0.97 for the slope and 0.002 for the offset.

The FMF value retrieved from each of the 560 TOA radiance sets using the synergistic retrieval method is compared with the true values in Fig. 4. The RMSE between true and estimated values is 0.11 and r^2 is 0.86. The regression coefficients are 0.93 for the slope and 0.04 for the offset.

The SSA values from the synergistic retrieval are compared with the true values in Fig. 5. The RMSE between true and estimated values is 0.02 and r^2 is 0.77. The regression coefficients are 0.88 for the slope and 0.11 for the offset.

An example of retrieved surface reflectance values from one of the 560 sets are displayed in Fig. 11, following successful aerosol retrieval. The simulated reflectances generated are marked in red and the retrieved reflectances are marked in blue, shown at all OLCI and SLSTR wavelengths.

5.2 AOD from CHRIS data

The results from the CHRIS images were analysed for image sets where there are AOD, FMF and SSA values to validate the retrieval (22 for AOD and FMF, 19 for SSA). However results show the spectral constraint does not provide information except over at least partially vegetated surfaces, and so a testing over a reduced set was also

performed, where image sets are rejected if the mean NDVI is less than 0.4. A second set of results are displayed with 9 image sets where the mean NDVI is greater than 0.4. For comparison, the AOD estimates from the original method Davies et al. (2010), which uses a version of the angular constraint only, and a standard 6S model set (Vermote et al., 1997a) are also displayed in Fig. 2.

5.2.1 All sites

The AOD value for each of the CHRIS image sets using only the angular method is compared with the ground based photometer readings in Fig. 6. The RMSE between photometer and CHRIS retrievals is 0.07 and r^2 is 0.58. The regression coefficients are 0.81 for the slope and 0.002 for the offset. The mean AOD for the CHRIS dataset is 0.09 for the 22 image sets which compares with the photometer mean AOD of 0.11.

The AOD value for each of the CHRIS image sets using only the spectral method is compared with the ground based photometer readings in Fig. 8. However over this dataset, no correlation is shown (r^2 is 0). The mean AOD for the CHRIS dataset is 0.13 for the 22 image sets which compares with the photometer mean AOD of 0.11.

The AOD value for each of the CHRIS image sets using the synergistic method is compared with the ground based photometer readings in Fig. 10. The RMSE between photometer and CHRIS retrievals is 0.06 and r^2 is 0.65 The regression coefficients are 0.90 for the slope and −0.008 for the offset. The mean AOD for the CHRIS dataset is 0.09 for the 22 image sets which compares with the photometer mean AOD of 0.11.

5.2.2 Vegetated sites

The AOD value for each of the screened CHRIS image sets where the mean NDVI is greater than 0.4 using only the angular method is compared with the ground based photometer readings in Fig. 7. The RMSE between photometer and CHRIS retrievals is 0.04 and r^2 is 0.86. The regression coefficients are 1.3 for the slope and −0.03 for

Title Page

Abstract | Introduction
Conclusions | References
Tables | Figures

Back | Close

Full Screen / Esc

Printer-friendly Version

Interactive Discussion

the offset. The mean AOD for the CHRIS dataset is 0.08 for the 9 image sets which compares with the photometer mean AOD of 0.09.

Using the spectral constraint only on this dataset shows The RMSE between photometer and CHRIS retrievals is 0.06 and r^2 is 0.44, shown in Fig. 9. The regression coefficients are 0.57 for the slope and 0.007 for the offset. The mean AOD for the CHRIS dataset is 0.06 for the 9 image sets which compares with the photometer mean AOD of 0.09.

Results for the synergistic constraint are shown in Fig. 14. The RMSE between photometer and CHRIS retrievals is 0.03 and r^2 is 0.89. The regression coefficients are 1.2 for the slope and −0.02 for the offset. The mean AOD for the CHRIS dataset is 0.08 for the 9 image sets which compares with the photometer mean AOD of 0.09.

An example of the retrieved multi-angle surface reflectance values (672 and 868 nm) from one of the image sets that passes the NDVI threshold test is shown in Fig. 12. The image set lg41c8 was aquired over Lake Argyle, Australia on 5 June 2004. The SZA is 44° and the Relative Azimuth (RA) ranges from −153° to +9°. The retrieved spectral surface reflectance values (nadir view) from a second image set that passes the NDVI threshold test are displayed in Fig. 13, along with the fitted reflectance from the mixture model. The image set ln3a16 was aquired over Lanai, Hawaii on 10 November 2003. The percentage of the various surface types in the model that gave the best fit for this Region Of Interest (ROI) were as follows: 94 % green vegetation, 4 % soil and 2 % dry grass. This ROI produced an overestimation of AOD (0.21 compared to an estimate of 0.06 from Aeronet). The spike is in the 760 nm oxygen absorption band.

5.3 FMF from CHRIS data

The FMF value for each of the CHRIS image sets, over the full dataset, calculated from the estimated mixture using the synergistic method is compared with the AERONET estimates in Fig. 15. The RMSE between photometer and CHRIS retrievals is 0.49 and r^2 is 0.05. The regression coefficients are −0.30 for the slope and 0.82 for the offset. The mean FMF for the CHRIS dataset is 0.65 for the 22 image sets which compares

with the photometer mean FMF of 0.59. Thresholding for high NDVI and optical depth yielded only 2 image sets suitable for testing – the image set from Gilching (gc) with the image id 415a resulted in an estimate for the FMF as 1.0 ± 0.13, compared to the Aeronet estimate of 0.82 ± 0.11. The image set from Mexico City (mc) with id 3ae3 gave a retrieved estimate of 1.0 ± 0.49 compared to Aeronet estimate of 0.85 ± 0.13.

5.4 SSA from CHRIS data

The SSA value for each of the CHRIS image sets, calculated from the estimated mixture using the synergistic method is compared with the AERONET estimates in Fig. 16, and shows no correlation, with an RMSE between photometer and CHRIS retrievals of 0.24. The mean SSA for the CHRIS dataset is 0.97 for the 19 image sets which compares with the photometer mean SSA of 0.80. Thresholding on high NDVI and optical depth yielded only one suitable site with Aeronet data, Mexico City (mc3ae3). Here the satellite retrieval estimated the SSA as 0.95 ± 0.63 compared to the Aeronet estimate of 0.77 ± 0.05.

6 Discussion

The results from the synergistic retrieval of AOD displayed in Fig. 10 show that this extended method is an improvement over the original method (Fig. 2) with an RMSE/r^2 of 0.06/0.65 compared to 0.09/0.60 for the original method.

The results from the spectral retrieval of AOD displayed in Fig. 8 show that the addition of spectral constraint does not provide useful information over all surface types. However, when the surface types are filtered to only include vegetation where the mean NDVI is greater than 0.4 the results are significantly better as seen in Figs. 9 and 14. This leads to an expectation that the real data will also benefit from filtering out of low NDVI scenes, where the angular constraint alone can provide a retrieval.

The poor results from the retrieval of FMF and SSA on the full dataset are consistent with the expectation that the filtering out of both low AOD and low NDVI scenes is required for retrieval of further aerosol properties than AOD. It should also be noted that the lowest possible SSA for 100 % strongly absorbing is 0.74 whereas 4 of the Aeronet estimates of SSA in this data set are below this value. Further research is recommended to identify CHRIS image sets that have a higher AOD and NDVI and to experiment with different values of refractive index for strongly absorbing aerosols. Finally it should be noted that only a subset of Sentinel-3 spectral bands were available from CHRIS, and improved results are expected by including wavebands beyond 1 μm.

7 Conclusions

A method for estimating AOD, FMF, SSA and their uncertainties from CHRIS/PROBA-1 images using Sentinel-3 bands for the spectral retrieval has been developed and tested on 22 image sets from 6 sites for AOD and FMF and 19 image sets from 5 sites for SSA. The method retrieves the mix of aerosol components using non-spherical dust, sea salt, weakly absorbing and strongly absorbing.

Estimates of AOD from this extended method with four unknowns and the improved aerosol models were compared to the AOD estimates using the standard 6S models with one unknown (Davies et al., 2010). The results are an improvement to the previous estimates with an RMSE of 0.06 and r^2 of 0.65 for the extended method, compared to 0.09 and 0.60 respectively for the previous method. The RMSE is 0.03 for the screened image sets where the mean NDVI is greater than 0.4 and the r^2 is 0.89. AOD from the simulated data has an RMSE of 0.03 and an r^2 of 0.97.

Results from simulated data show an RMSE of 0.11 and r^2 is 0.86 for FMF and an RMSE of 0.02 in SSA with an r^2 of 0.77 from 560 TOA radiance sets, with results improving at higher optical depth. However results from CHRIS data over the full dataset do not show correlation between retrieved FMF and SSA with Aeronet values. Screened image data did not yield sufficient number of points to reliably test the

Discussion Paper | Discussion Paper | Discussion Paper | Discussion Paper | Discussion Paper

retrieval of aerosol properties. Further research is therefore recommended to examine the retrieval of aerosol propreties over higher AOD values and over vegetated surfaces, and to explore the performance using different models of aerosol aerosol properties and surface spectra.

References

Ackerman, A. S., Toon, O. B., Stevens, D. E., Heymsfield, A. J., Ramanathan, V., and Welton, E. J.: Reduction of tropical cloudiness by soot, Science, 288, 1042–1047, 2000. 5383
15 Baldridge, A. M., Hook, S. J., Grove, C. I., and Rivera, G.: The ASTER spectral library version 2.0, Remote Sens. Environ., 113, 711–715, 2009. 5387, 5404, 5405
Bergstrom, R. W., Russell, P. B., and Hignett, P.: Wavelength dependence of the absorption of black carbon particles: predictions and results from the TARFOX experiment and implications for the aerosol single scattering albedo, J. Atmos. Sci., 59, 567–577, 2002. 5383
20 Bevan, S. L., North, P. R., Los, S. O., and Grey, W. M.: A global dataset of atmospheric aerosol optical depth and surface reflectance from AATSR, Remote Sens. Environ., 116, 199–210, 2012. 5383
Cutter, M. A.: CHRIS Data Format, Sira Technology Ltd., Kent, UK, 4.2 edn., 2005. 5402
Cutter, M. A. and Lobb, D. R.: Design of the compact high-resolution imaging spectrometer (CHRIS), and future developments, available at: http://envisat.esa.int/pub/ESA_DOC/
25 PROBA/Sira5thICSO2004CHRISpaperSP-554.PDF (last access: 25 April 2014), 2004. 5386

Synergistic aerosol estimation from simulated Sentinel-3 data

W. H. Davies and P. R. J. North

Davidson, M. and Vuilleumier, P.: Note on CHRIS acquisition procedure and image geometry, available at: http://earth.esa.int/pub/ESA_DOC/CHRIS_acquisition-procedure_image-geometry_rev1_3.pdf (last access: 25 April 2014), 2004. 5386

Davies, W. H., North, P. R. J., Grey, W. M. F., and Barnsley, M. J.: Improvements in aerosol optical depth estimation using multiangle CHRIS/PROBA images, IEEE T. Geosci. Remote, 48, 18–24, 2010. 5383, 5385, 5386, 5389, 5392, 5394, 5397

de Leeuw, G., Holzer-Popp, T., Bevan, S. L., Davies, W. H., Descloitres, J., Graigner, R. G., Griesfeller, J., Heckel, A., von Hoyningen Huene, W., Kinne, S., Klüser, L., Kolmonen, P., Litvinov, P., Martynenko, D., North, P. R. J., Ovigneur, B., Poulsen, C. A., Ramon, D., Schulz, M., Siddans, R., Sogacheva, L., Tanré, D., Thomas, G. E., Timo, H., Vountas, M., and Pinnock, S.: Evaluation of seven European aerosol optical depth retrieval algorithms for climate analysis, Remote Sens. Environ., doi:10.1016/j.rse.2013.04.023, online first, 2013. 5383, 5388, 5390, 5403

Diner, D. J., Abdou, W., Ackerman, T. P., Crean, K., Gordon, H. R., Kahn, R. A., Martonchik, J. V., McMuldroch, S., Paradise, S. R., Pinty, B., Verstraete, M. M., Wang, M., and West, R. A.: MISR Level 2 Aerosol Retrieval Algorithm Theoretical Basis, available at: http://eospso.gsfc.nasa.gov/eos_homepage/for_scientists/atbd/docs/MISR/atbd-misr-09.pdf (last access: 25 April 2014), 2008. 5390, 5391

Donlon, C., Berruti, B., Buongiorno, A., Ferreira, M.-H., Féménias, P., Frerick, J., Goryl, P., Klein, U., Laur, H., Mavrocordatos, C., Nieke, J., Rebhan, H., Seitz, B., Stroede, J., and Sciarra, R.: The Global Monitoring for Environment and Security (GMES) Sentinel-3 mission, Remote Sens. Environ., 120, 37–57, 2012. 5383, 5384, 5385, 5402

Dubovik, O., Holben, B. N., Eck, T. F., Smirnov, A., Kaufman, Y. J., King, M. D., Tanré, D., and Slutsker, I.: Variability of absorption and optical properties of key aerosol types observed in worldwide locations, J. Atmos. Sci., 59, 590–608, 2002. 5383

ESA-Earth-Online: Sentinel-3, available at: http://earth.esa.int/web/guest/missions/esa-future-missions/sentinel-3 (last access: 5 March 2014), 2014. 5383

GCOS, G. C. O. S.: Systematic Observation Requirements for Satellite-based Products for Climate, available at: http://www.wmo.int/pages/prog/gcos/Publications/gcos-107.pdf (last access: 5 March 2014), 2006. 5382

Gómez-Chova, L., Alonso, L., Guanter, L., Camps-Valls, G., Calpe, J., and Moreno, J.: Correction of systematic spatial noise in push-broom hyperspectral sensors: application to CHRIS/PROBA images, Appl. Optics, 47, F46–F60, 2008. 5386

Synergistic aerosol estimation from simulated Sentinel-3 data

W. H. Davies and P. R. J. North

Title Page

Abstract	Introduction
Conclusions	References
Tables	Figures

|◄ | ►|

◄ | ►

Back | Close

Full Screen / Esc

Printer-friendly Version

Interactive Discussion

Guanter, L., Alonso, L., and Moreno, J.: A method for the surface reflectance retrieval from PROBA/CHRIS data over land: application to ESA SPARC campaigns, IEEE T. Geosci. Remote, 43, 2908–2917, 2005. 5387

Holzer-Popp, T., de Leeuw, G., Griesfeller, J., Martynenko, D., Klüser, L., Bevan, S., Davies, W., Ducos, F., Deuzé, J. L., Graigner, R. G., Heckel, A., von Hoyningen-Hüne, W., Kolmonen, P., Litvinov, P., North, P., Poulsen, C. A., Ramon, D., Siddans, R., Sogacheva, L., Tanre, D., Thomas, G. E., Vountas, M., Descloitres, J., Griesfeller, J., Kinne, S., Schulz, M., and Pinnock, S.: Aerosol retrieval experiments in the ESA Aerosol_cci project, Atmos. Meas. Tech., 6, 1919–1957, doi:10.5194/amt-6-1919-2013, 2013. 5382, 5383

IPCC: Climate Change 2013: The Physical Science Basis. Contribution of Working Group I to the Fifth Assessment Report of the Intergovernmental Panel on Climate Change, edited by: Stocker, T. F., Qin, D., Plattner, G. K., Tignor, M., Allen, S. K., Boschung, J., Nauels, A., Xia, Y., Bex, V., and Midgley, P. M., Cambridge University Press, Cambridge, UK, New York, NY, USA, 2013. 5382, 5383

Kazadzis, S., Gröbner, J., Arola, A., and Amiridis, V.: The effect of the global UV irradiance measurement accuracy on the single scattering albedo retrieval, Atmos. Meas. Tech., 3, 1029–1037, doi:10.5194/amt-3-1029-2010, 2010. 5383

Kokhanovsky, A. A. and DeLeeuw, G.: Satellite Aerosol Remote Sensing over Land, Springer Praxis Books, Heidelberg, 2009. 5383

Kokhanovsky, A. A., Deuzé, J. L., Diner, D. J., Dubovik, O., Ducos, F., Emde, C., Garay, M. J., Grainger, R. G., Heckel, A., Herman, M., Katsev, I. L., Keller, J., Levy, R., North, P. R. J., Prikhach, A. S., Rozanov, V. V., Sayer, A. M., Ota, Y., Tanré, D., Thomas, G. E., and Zege, E. P.: The inter-comparison of major satellite aerosol retrieval algorithms using simulated intensity and polarization characteristics of reflected light, Atmos. Meas. Tech., 3, 909–932, doi:10.5194/amt-3-909-2010, 2010. 5383

North, P. and Heckel, A.: Sentinel-3 L2 Products and Algorithm Definition: SYN Algorithm Theoretical Basis Document S3-L2-SD-03-S02-ATBD, available at: https://earth.esa.int/documents/247904/349589/SYN_L2-3_ATBD.pdf (last access: 28 May 2014), 2012. 5384

North, P., Brockmann, C., Fischer, J., Gomez-Chova, L., Grey, W., Heckel, A., Moreno, J., Preusker, R., and Regner, P.: MERIS/AATSR synergy algorithms for cloud screening, aerosol retrieval and atmospheric correction, Proc. 2nd MERIS/AATSR User Workshop, ESRIN, Frascati, 22–26, 2008. 5384, 5387

Synergistic aerosol estimation from simulated Sentinel-3 data

W. H. Davies and P. R. J. North

Title Page

Abstract | Introduction

Conclusions | References

Tables | Figures

|◄ | ►|

◄ | ►

Back | Close

Full Screen / Esc

Printer-friendly Version

Interactive Discussion

North, P., Grey, W., Heckel, A., Fischer, J., Preusker, R., and Brockmann, C.: MERIS/AATSR Synergy: Land Aerosol and Surface Reflectance Algorithm Theoretical Basis Document (ATBD), available at: http://github.com/downloads/bcdev/beam-meris-aatsr-synergy/synergy-land_aerosol-atbd.pdf (last access: 28 May 2014), 2010. 5384

North, P. R. J.: Estimation of aerosol opacity and land surface bidirectional reflectance from ATSR-2 dual-angle imagery: operational method and validation, J. Geophys. Res., 107, doi:10.1029/2000JD000207, AAC4-1–AAC4-10, 2002. 5383

North, P. R. J., Briggs, S. A., Plummer, S. E., and Settle, J. J.: Retrieval of land surface bidirectional reflectance and aerosol opacity from ATSR-2 multi-angle imagery, IEEE T. Geosci. Remote, 37, 526–537, 1999. 5386

Press, W. H., Teukolsky, S. A., Vetterling, W. T., and Flannery, B. P.: Numerical Recipes in C, The Art of Scientific Computing (Second Edition), Cambridge University Press, Cambridge, 1992. 5390

Vermote, E. F., Tanré, D., Deuzé, J. L., Herman, M., and Morcette, J. J.: Second simulation of the satellite signal in the solar spectrum, 6S: an overview, IEEE T. Geosci. Remote, 35, 675–686, 1997a. 5384, 5386, 5387, 5394, 5404, 5405

Vermote, E. F., Tanré, D., Deuzé, J. L., Herman, M., and Morcette, J. J.: Second simulation of the satellite signal in the solar spectrum, 6S: Users Guide, Laboratoire d'Optique Atmospherique, U. S. T. de Lille, 59655 Villeneuve d'Aseq, France, 2 edn., 1997b. 5388

von Hoyningen-Huene, W., Yoon, J., Vountas, M., Istomina, L. G., Rohen, G., Dinter, T., Kokhanovsky, A. A., and Burrows, J. P.: Retrieval of spectral aerosol optical thickness over land using ocean color sensors MERIS and SeaWiFS, Atmos. Meas. Tech., 4, 151–171, doi:10.5194/amt-4-151-2011, 2011. 5387

Title Page

Abstract | Introduction

Conclusions | References

Tables | Figures

◄ | ►

◄ | ►

Back | Close

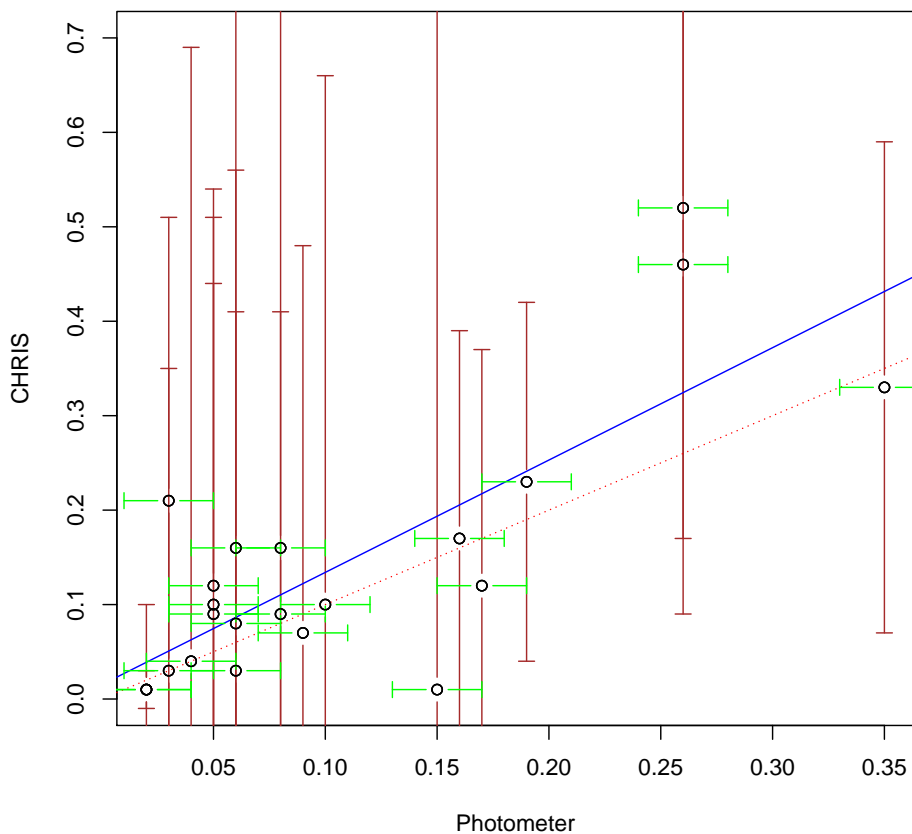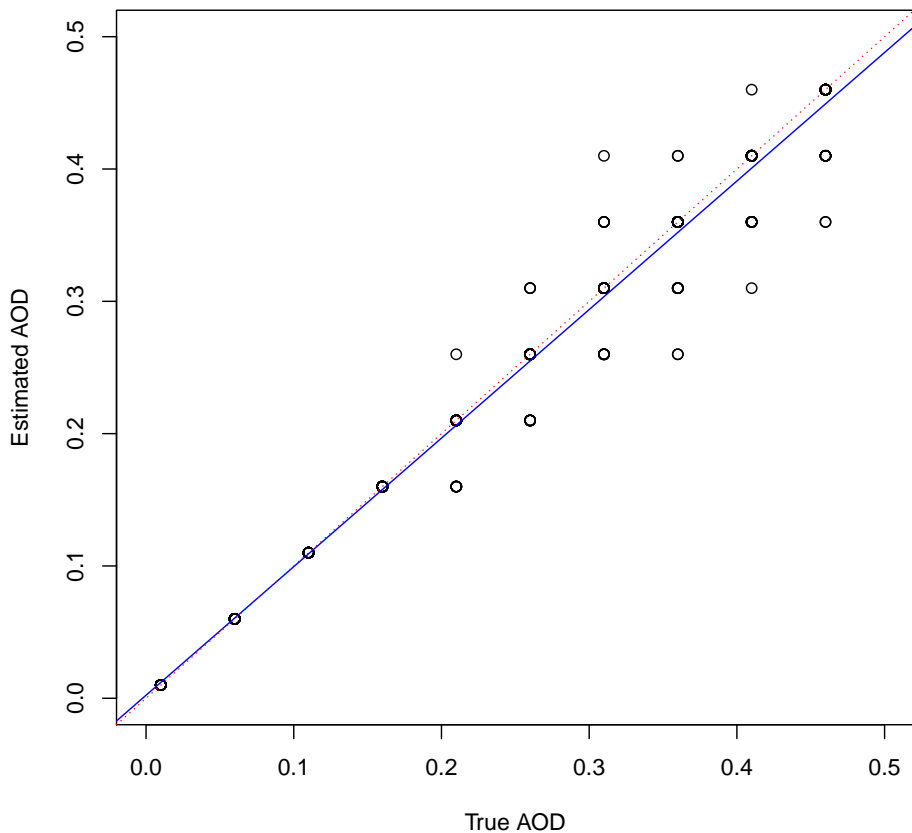Full Screen / Esc

Printer-friendly Version

Interactive Discussion

Table 1. Wavelength bands used (µm) (Donlon et al., 2012; Cutter, 2005).

SLSTR	OLCI	CHRIS Mode 1	CHRIS Mode 5
	0.3925 0.4075		
	0.4075 0.4175	0.406 0.415	
	0.4375 0.4475	0.438 0.447	0.438 0.447
	0.485 0.495	0.486 0.495	0.486 0.495
		0.495 0.505	
	0.505 0.515	0.505 0.515	
			0.526 0.534
0.540 0.560	0.555 0.565	0.556 0.566	0.546 0.556
			0.566 0.573
	0.615 0.625	0.618 0.627	
			0.627 0.636
	0.660 0.670	0.656 0.666	0.656 0.666
0.655 0.675	0.670 0.6775	0.666 0.677	0.666 0.677
	0.6775 0.685	0.677 0.683	0.677 0.689
	0.70375 0.71375	0.706 0.712	0.706 0.712
	0.750 0.7575	0.752 0.759	0.752 0.759
	0.760 0.7625	0.759 0.766	0.759 0.766
	0.77125 0.78625	0.773 0.781	0.773 0.788
0.855 0.875	0.855 0.875	0.863 0.872	0.863 0.881
	0.880 0.890	0.881 0.891	0.881 0.891
	0.895 0.905	0.900 0.910	0.900 0.910
		0.981 0.992	0.981 0.992
	1.000 1.040		1.003 1.036
1.580 1.640			
2.225 2.275			

Title Page

Abstract | Introduction

Conclusions | References

Tables | Figures

|◄ | ►|

◄ | ►

Back | Close

Full Screen / Esc

Printer-friendly Version

Interactive Discussion

Table 2. Log-normal parameters for the aerosol components (de Leeuw et al., 2013).

Aerosol Component	Real Index of Refraction (0.55 µm)	Imaginary Index of Refraction (0.55 µm)	Effective Radius (µm)	Geometric Standard Deviation
Dust	1.56	0.0018	1.94	1.822
Sea Salt	1.4	0	1.94	1.822
Weakly absorbing	1.4	0.003	0.14	1.7
Strongly absorbing	1.5	0.040	0.14	1.7

Table 3. OLCI spectra (Baldridge et al., 2009; Vermote et al., 1997a).

Wavelength (µm)	ρ_{vg}	ρ_{vd}	ρ_{vo}	ρ_s	ρ_a
0.400000	0.046470	0.157013	0.045815	0.036768	0.029020
0.412500	0.047242	0.170558	0.063035	0.049469	0.038720
0.442500	0.049020	0.199196	0.076099	0.073796	0.062344
0.490000	0.052483	0.241431	0.106535	0.107402	0.103530
0.510000	0.064435	0.259522	0.121465	0.122475	0.123760
0.560000	0.103197	0.313778	0.121022	0.182937	0.194380
0.620000	0.061505	0.372506	0.077998	0.254738	0.267570
0.665000	0.045183	0.419670	0.104285	0.283098	0.289420
0.673750	0.044693	0.430844	0.161134	0.287909	0.300673
0.681250	0.047156	0.440263	0.206083	0.294213	0.299675
0.708750	0.176344	0.471079	0.377132	0.310058	0.321040
0.753750	0.482001	0.510188	0.519670	0.334321	0.336595
0.761250	0.492245	0.515876	0.520708	0.336472	0.337490
0.778750	0.503628	0.525009	0.523003	0.345266	0.343143
0.865000	0.523376	0.575062	0.529749	0.361608	0.348803
0.885000	0.525212	0.585798	0.530996	0.365007	0.352213
0.900000	0.525729	0.594547	0.532001	0.367217	0.351690
1.020000	0.518955	0.637942	0.530199	0.397384	0.378390

Table 4. CHRIS spectra (Baldridge et al., 2009; Vermote et al., 1997a).

Wavelength (µm)	ρ_{vg}	ρ_{vd}	ρ_{vo}	ρ_s	ρ_a
0.410500	0.047118	0.168391	0.062435	0.047437	0.035117
0.442000	0.048990	0.198719	0.075873	0.073391	0.062389
0.490000	0.052483	0.241431	0.106638	0.107402	0.103530
0.500000	0.058459	0.250477	0.114682	0.114938	0.115380
0.510000	0.064435	0.259522	0.121645	0.122475	0.123760
0.561000	0.102502	0.314757	0.120774	0.184134	0.194920
0.622000	0.060780	0.374602	0.077075	0.255998	0.265680
0.661000	0.046634	0.415478	0.083445	0.280577	0.290130
0.672000	0.044791	0.428609	0.143919	0.286947	0.294930
0.680000	0.046746	0.438693	0.198597	0.293162	0.298620
0.709000	0.178042	0.471296	0.371412	0.310193	0.318970
0.755500	0.484391	0.511515	0.520058	0.334823	0.336180
0.762500	0.493058	0.516031	0.521425	0.337100	0.338945
0.777000	0.502490	0.523939	0.521732	0.344387	0.344520
0.867500	0.523605	0.576404	0.530533	0.362033	0.348741
0.886000	0.525246	0.586381	0.531138	0.365154	0.352515
0.905000	0.525447	0.597530	0.531993	0.368474	0.353335
0.986500	0.518940	0.629763	0.536559	0.388962	0.367166

Table 5. CHRIS sites and image sets.

Site	Sets	Land cover	Model	Date range	AOD range
Tinga Tingana (Aus)	8	Arid	Desertic	Dec 2003–Nov 2006	0.02–0.10
Lake Argyle (Aus)	8	Semi-arid	Continental	Jun 2003–Apr 2007	0.02–0.35
Great Plains (USA)	2	Agricultural	Continental	Oct 2003–May 2004	0.03–0.08
Mexico City (Mex)	2	Urban	Urban	Nov 2003–Dec 2003	0.26
Lanai (USA)	1	Shrublands	Maritime	Nov 2003	0.06
Gilching (Ger)	1	Agricultural	Continental	May 2004	0.16
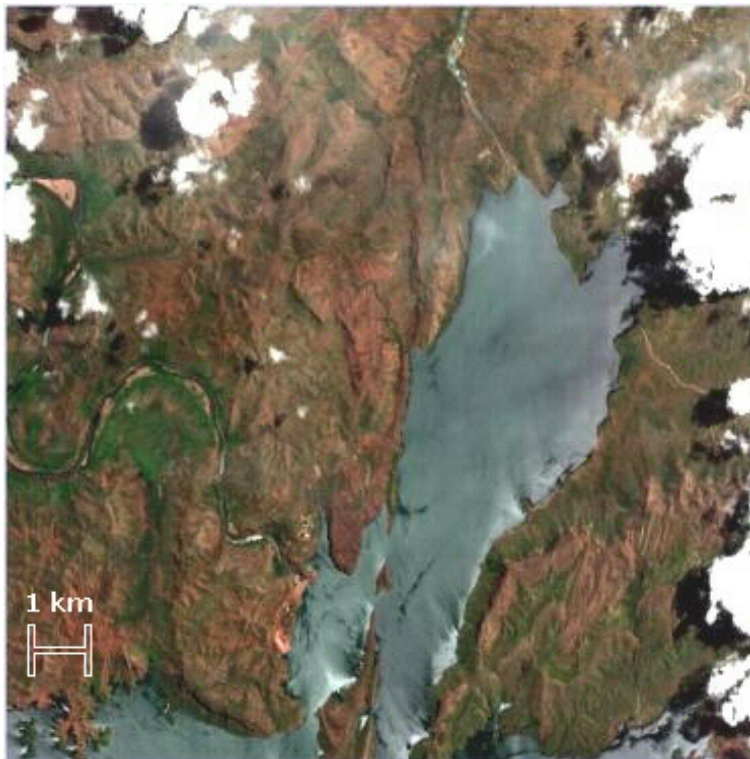
Figure 1. True Colour Nadir CHRIS image of lg3e35, Lake Argyle, Australia. 16.11° S, 128.75° E (© Surrey Satellite Technology Ltd.).

Figure 2. AOD from original method.

Figure 3. AOD comparison for synergistic retrieval from simulated SLSTR and OLCI data.
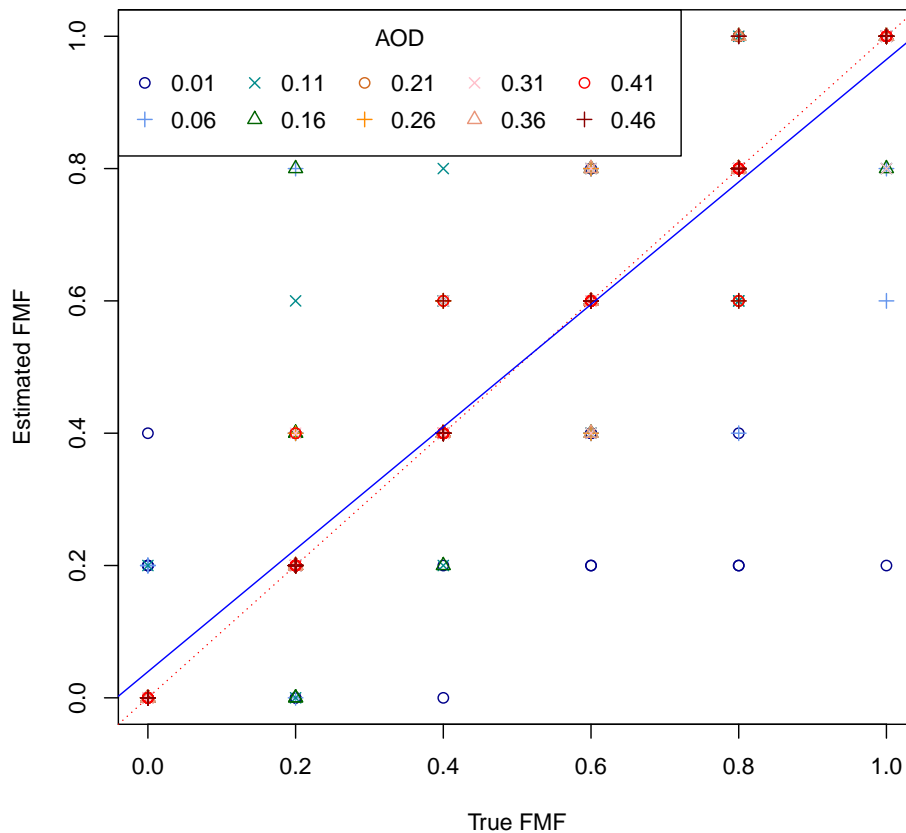
Figure 4. Simulated FMF vs. estimated FMF categorised by AOD from synergistic retrieval.
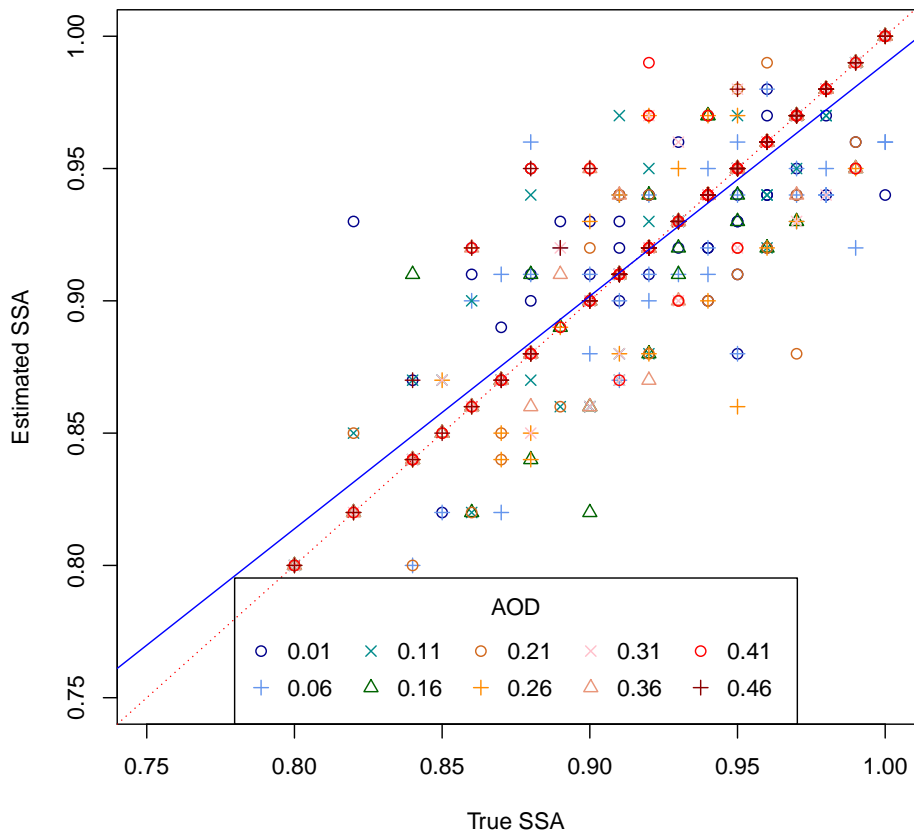
Figure 5. Simulated SSA vs. estimated SSA categorised by AOD from synergistic retrieval.
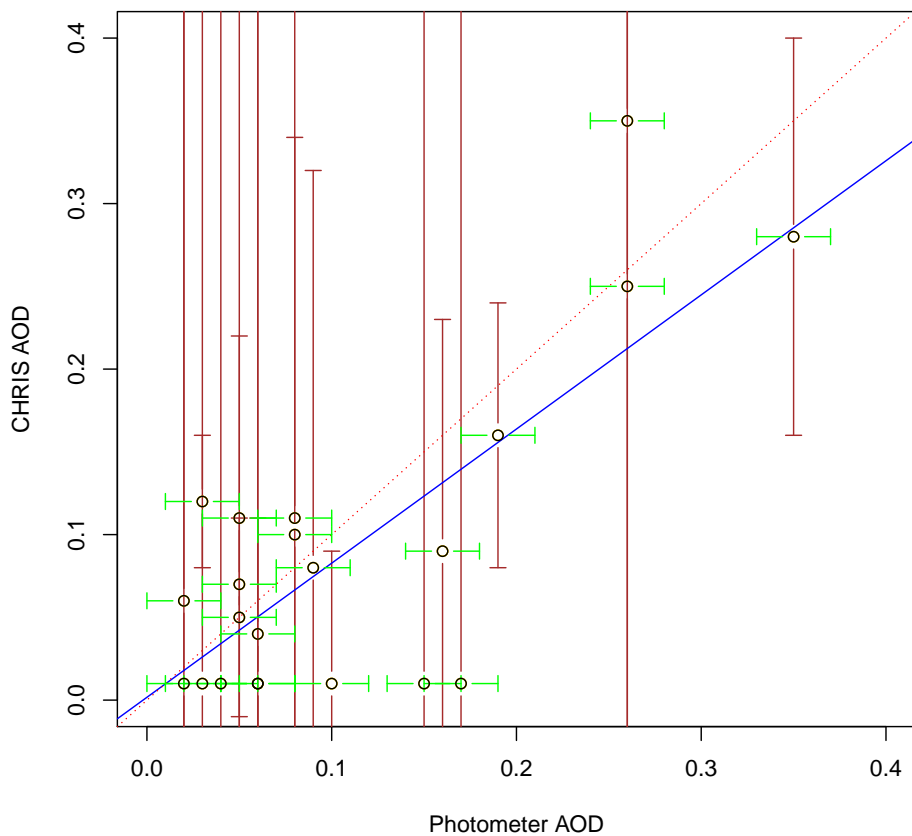
Figure 6. AOD comparison for angular retrieval from CHRIS data.
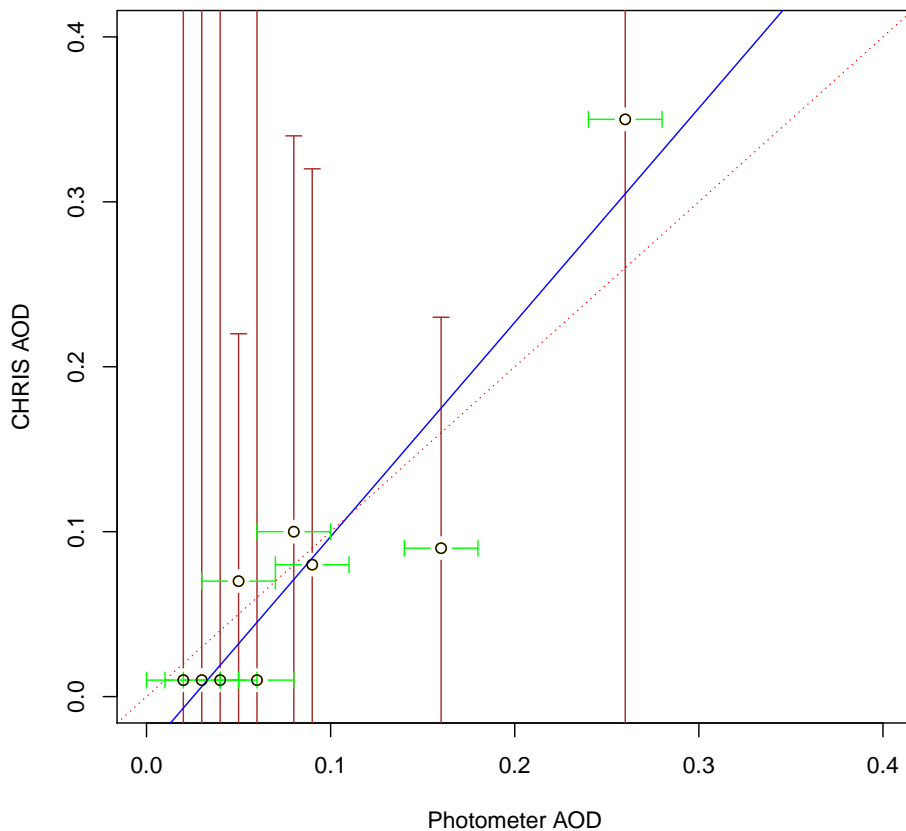
Figure 7. AOD comparison for angular retrieval from CHRIS data where the mean NDVI > 0.4.
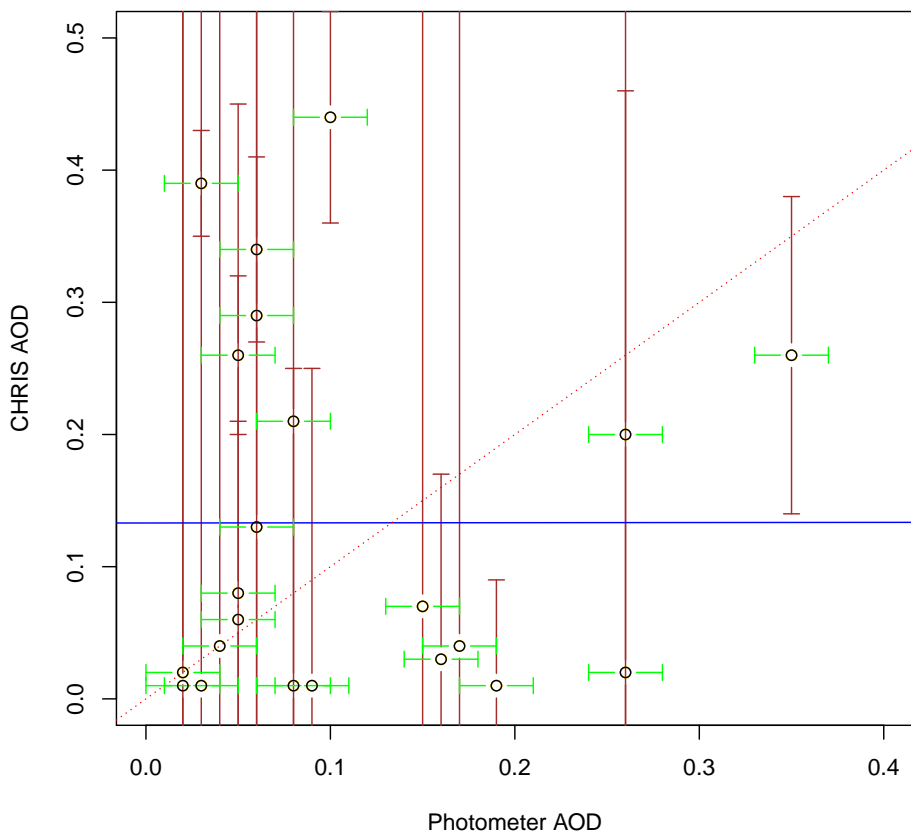
Figure 8. AOD comparison for spectral retrieval from CHRIS data.
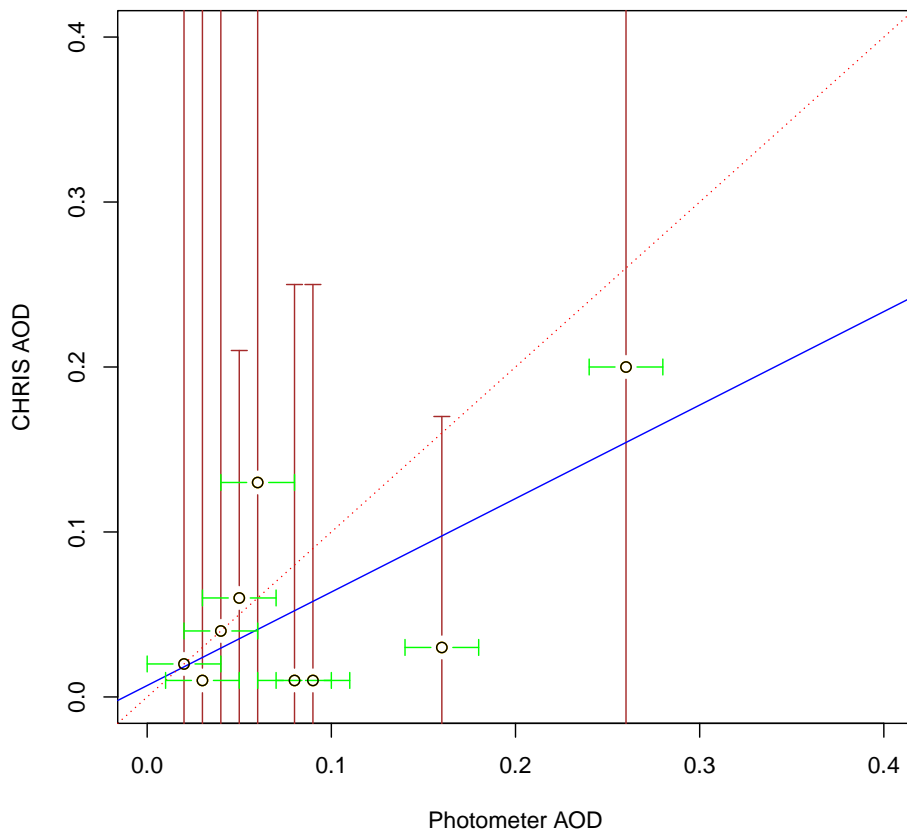
Figure 9. AOD comparison for spectral retrieval from CHRIS data where the mean NDVI > 0.4.
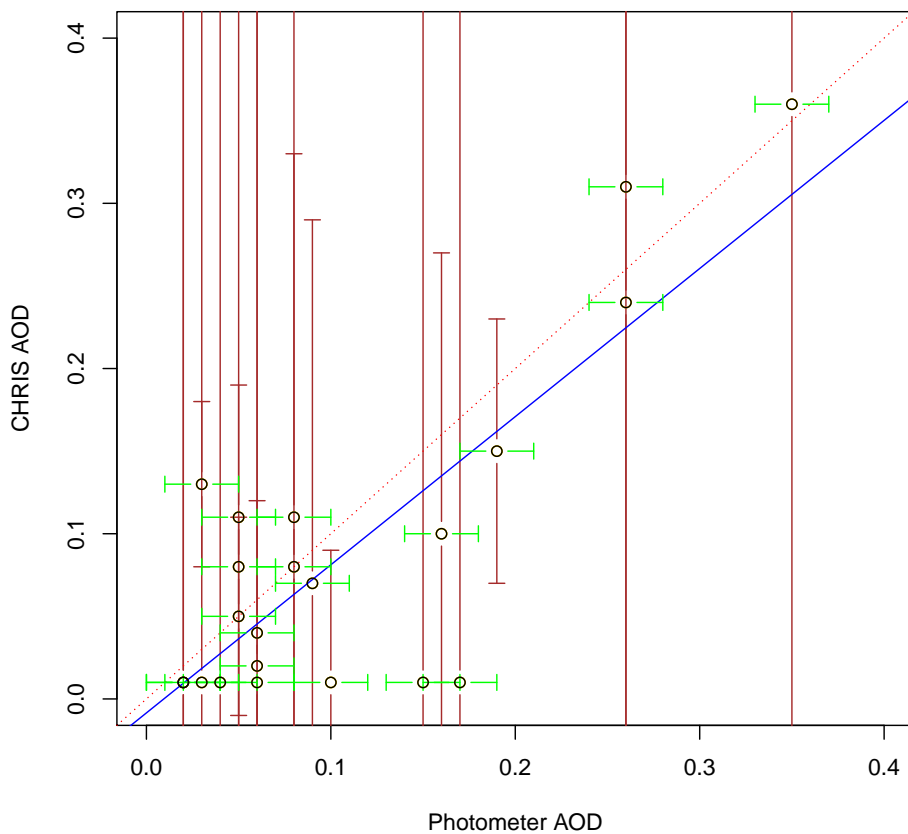
Figure 10. AOD comparison for synergistic retrieval from CHRIS data.

Printer-friendly Version

Interactive Discussion
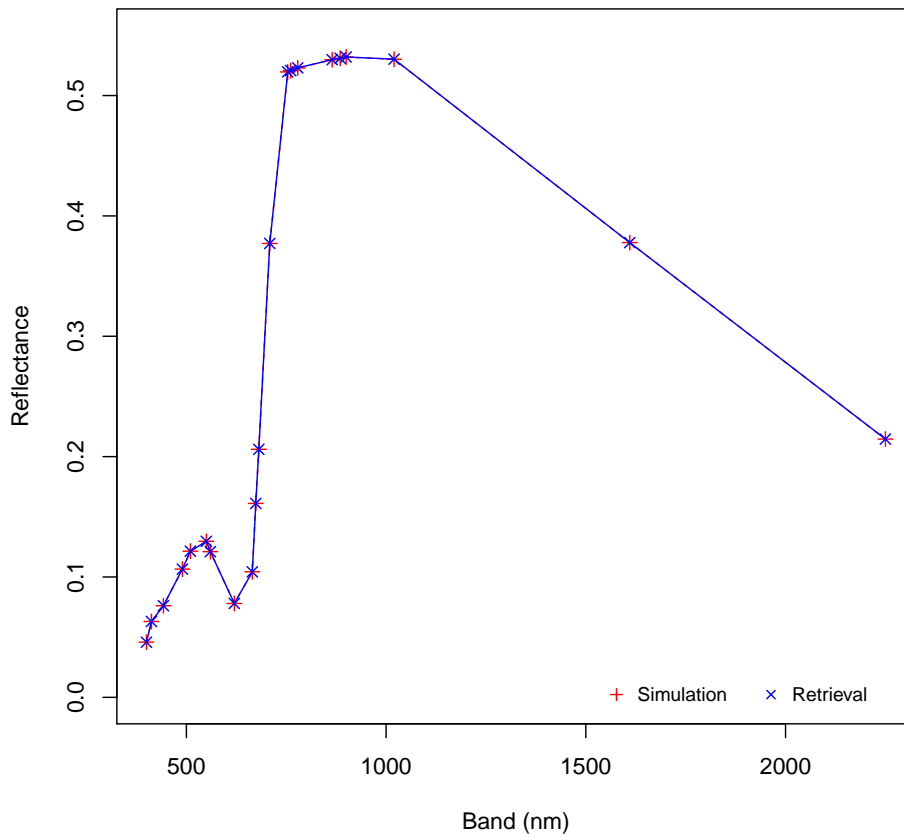
Figure 11. Retrieved surface reflectance from simulated SLSTR and OLCI data (AOD = 0.46, 100 % dust).
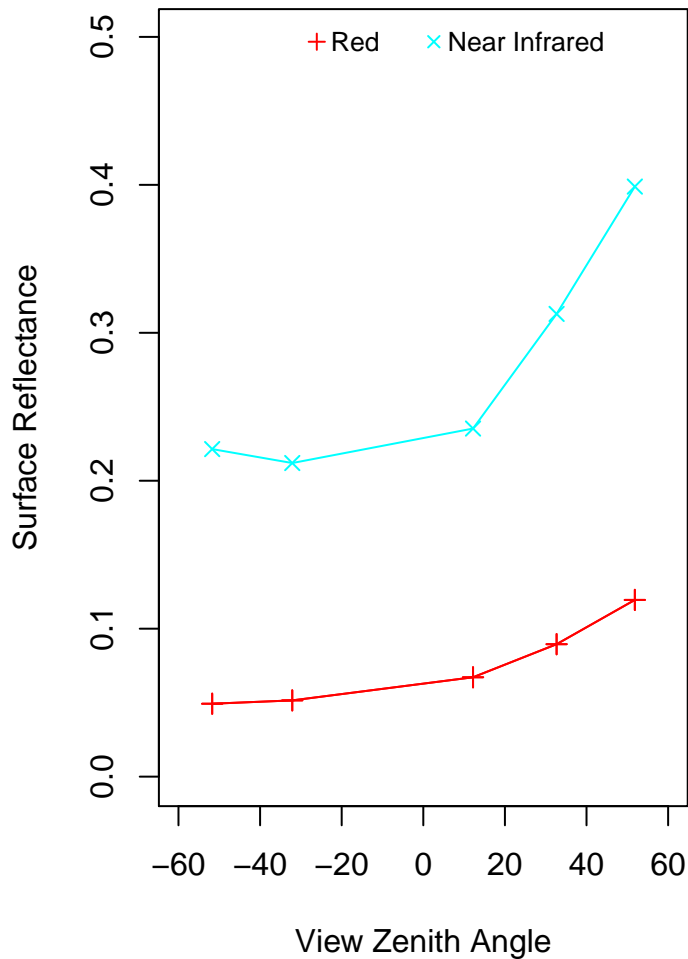
Figure 12. Retrieved multi-angle surface reflectance from CHRIS image set lg41c8.

Figure 13. Retrieved spectral surface reflectance from CHRIS image set ln3a16.

Title Page

Abstract | Introduction

Conclusions | References

Tables | Figures

◄ | ►

◄ | ►

Back | Close

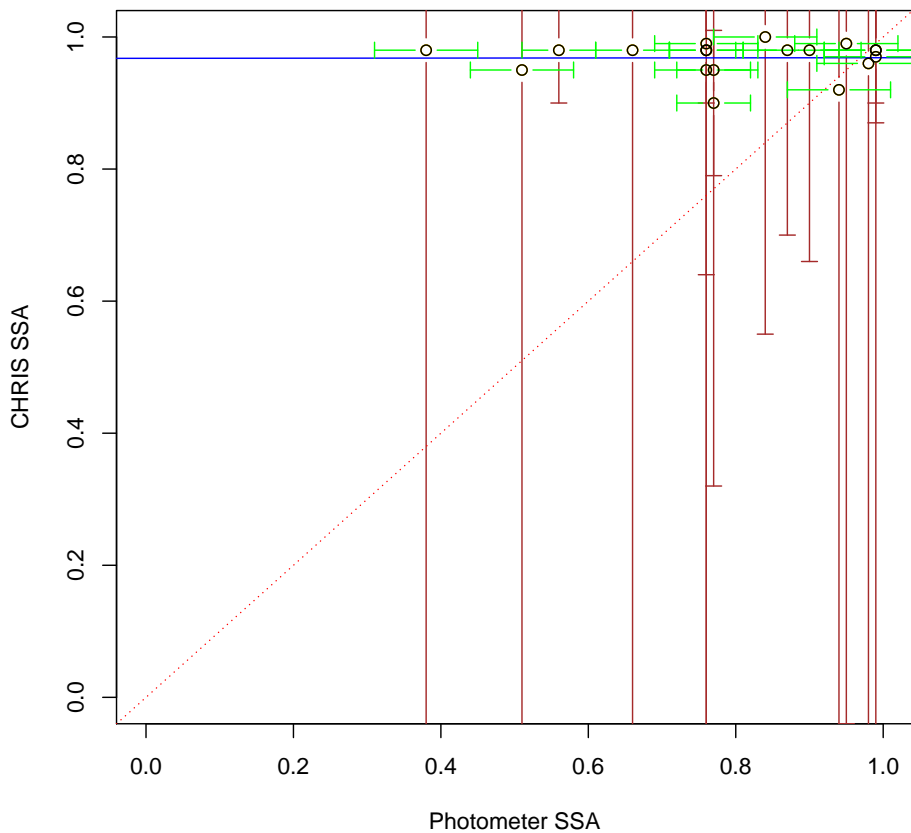Full Screen / Esc

Printer-friendly Version

Interactive Discussion

Figure 14. AOD comparison for synergistic retrieval from CHRIS data where the mean NDVI > 0.4.

Figure 15. FMF comparison for synergistic retrieval from CHRIS data.

Figure 16. SSA comparison for synergistic retrieval from CHRIS data.